Spin-mediated Mott excitons

T.-S. Huang, C. L. Baldwin, M. Hafezi, and V. Galitski

Spin-mediated Mott excitons

T.-S. Huang,[1,2] C. L. Baldwin,[1,3] M. Hafezi,[1] and V. Galitski[1,2]

[1]*Joint Quantum Institute, University of Maryland, College Park, MD 20742, USA*
[2]*Condensed Matter Theory Center, University of Maryland, College Park, MD 20742, USA*
[3]*National Institute of Standards and Technology, Gaithersburg, MD 20899, USA*
(Dated: January 5, 2023)

Motivated by recent experiments on Mott insulators, in both iridates and ultracold atoms, we theoretically study the effects of magnetic order on the Mott-Hubbard excitons. In particular, we focus on spin-mediated doublon-holon pairing in Hubbard materials. We use several complementary theoretical techniques: mean-field theory to describe the spin degrees of freedom, the self-consistent Born approximation to characterize individual charge excitations across the Hubbard gap, and the Bethe-Salpeter equation to identify bound states of doublons and holons. The binding energy of the Mott exciton is found to increase with increasing the Néel order parameter, while the exciton mass decreases. We observe that these trends rely significantly on the retardation of the effective interaction, and require consideration of multiple effects from changing the magnetic order. Our results are consistent with the key qualitative trends observed in recent experiments on iridates. Moreover, the findings could have direct implications on ultracold atom Mott insulators, where the Hubbard model is the exact description of the system and the microscopic degrees of freedom can be directly accessed.

I. INTRODUCTION

The physics of excitons in semiconductors, i.e., bound states of electrons and holes, is by now well-established [1, 2]. Excitons play an essential role in technologies such as light-emitting diodes [3], organic solar cells [4], and photodetectors [5], among others. Furthermore, there has recently been tremendous interest in hybridizing exciton states with photon modes in optical cavities [6]. Such exciton polaritons can form (non-equilibrium) Bose-Einstein condensates at remarkably high temperatures, even room temperature [7–11].

Given these applications, it is important to study the properties of excitons in systems other than conventional semiconductors. It has been convincingly established that excitonic states do exist in strongly correlated materials such as Mott insulators [12–28], yet essential aspects of Mott excitons remain poorly understood.

For example, it is known that Mott insulators are often antiferromagnetic at low temperature, but very little work has been done to understand how and to what extent the presence of such order affects exciton properties. The qualitative role of magnetization is sketched in Fig. 1 – charges remain bound so as to minimize the number of spins disrupted by their motion – but a quantitative description has been lacking.

Recent experiments have begun to investigate this question. In Refs. [29, 30], pump-probe experiments were performed on the Mott insulator Na_2IrO_3 both with and without magnetic order (controlled by varying temperature or applying an intermediate pulse). The authors concluded that the binding energy and exciton mass are both enhanced by the presence of magnetization. Ref. [31] similarly observed that the binding energy increases with the spin-spin interaction strength in cuprates. See also Ref. [32], which found that the relaxation time in Mott insulators decreases with increasing
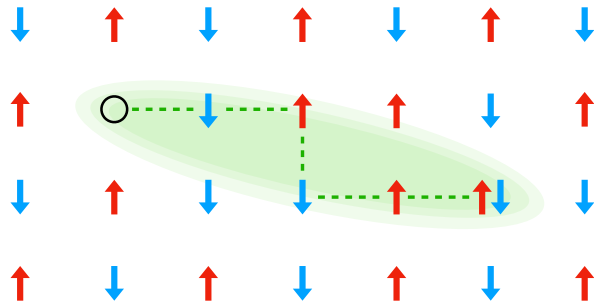

FIG. 1. Sketch of the physics underlying spin-mediated exciton formation in a Mott insulator. A string of flipped spins (green line) connects the hole and double-occupancy. The energy cost associated to the string binds them together.

spin correlations.

The same question can apply to Mott insulators in synthetic quantum systems, such as ultracold gases. By loading fermionic atoms into an optical lattice and tuning their interactions, the Fermi-Hubbard model can be synthesized experimentally [33–37]. Unlike condensed matter systems such as the iridates and cuprates, for which the Hubbard model is a significant idealization, neutral fermionic atoms in an optical lattice are genuinely described by the Hubbard Hamiltonian, without any additional effects arising from longer-range Coulomb interactions, phonons, etc. Researchers have quite recently begun investigating the interplay of spin and charge degrees of freedom in this setting [38–44] (note that here the "charge" excitations are not actually charged).

In this paper, we perform a theoretical study of the role of magnetic order in Mott excitons, the first such to our knowledge. As depicted in Fig. 1, in an antiferromagnetic background, a hole and doubly occupied site can bind through a string of flipped spins. Such

Mott excitons differ from conventional excitons formed by Coulomb interaction in two aspects. First, the spin-mediated interaction is far from instantaneous, and second, the individual charges are themselves renormalized by spin fluctuations. We shall demonstrate that both effects are necessary ingredients in the trends reported here.

Given the complexity of the problem, our analysis requires multiple stages. We first use slave particles to isolate spin and charge degrees of freedom, then describe the spin dynamics by mean-field theory, calculate the dispersion of charges self-consistently, and finally characterize excitonic states via the Bethe-Salpeter equation. Many of the steps in this program are analogous to those in Ref. [45], which studied charge dynamics in the Hubbard model. The good agreement between the results of Ref. [45] and alternate numerical methods lends support to the present approach.

Our key finding is that larger magnetization leads to an increased binding energy of the Hubbard exciton but a decreased mass. This observation is in some tension with interpretations of recent experiments [30]. It also stands in contrast to conventional Coulomb-mediated excitons, where the binding energy and mass are proportional to each other.

Note that the formation of Mott excitons is closely related to the Cooper pairing of holes in high-T_c superconductors. Similar treatments of hole-hole binding can be found in the corresponding literature [46–50]. Nonetheless, there are differences between the two problems, as we discuss below. Moreover, to the best of our knowledge, a study of how the bound state properties change as a function of magnetization has not yet been carried out.

In the following Sec. II, we describe the steps of our analysis in detail. Results are presented in Sec. III, and Sec. IV concludes.

II. FORMALISM & METHODS

Our starting point is the 2D Fermi-Hubbard model, which by now needs no introduction:

$$H_{\text{Hub}} = -t \sum_{\langle ij \rangle, \sigma} c_{i\sigma}^\dagger c_{j\sigma} + U \sum_i n_{i\uparrow} n_{i\downarrow}, \qquad (1)$$

where $\sigma \in \{\uparrow, \downarrow\}$ and $\langle ij \rangle$ denotes nearest-neighbor sites on a square lattice. $c_{i\sigma}$ is the usual electron annihilation operator and $n_{i\sigma} \equiv c_{i\sigma}^\dagger c_{i\sigma}$. We shall consider the system at half filling in the $U \gg t$ limit. While admittedly an idealization, especially for strongly correlated materials, Eq. (1) already exhibits a wide range of interesting phenomena.

It is well-known that in the large-U limit, the Hubbard model features two types of excitations, associated with the transport of charge and spin respectively [51–54]. Furthermore, the charge excitations can be either

positive or negative, corresponding to sites with zero or two electrons, and their creation comes with a large energy cost of order U. By analogy with conventional semiconductors, we thus expect this system to support well-defined excitons in the dilute-charge limit. However, long-wavelength spin excitations do not come with an energy cost, and their presence plays a significant role in determining the exciton properties.

There are many formalisms with which to study the Hubbard model [28, 55–58]. Since our focus is on the motion of only a few charges within a background of spin excitations, the slave-particle formalism is particularly well-suited [45, 59, 60]. The steps of our calculation are as follows:

i) Express the Hamiltonian in terms of slave particles – doublons, holons, & spinons – and reduce to the t-J model following the standard procedure [61].

ii) Treat the Heisenberg interaction within semiclassical and mean-field approximations, while neglecting the back action of doublons and holons on the magnetic order.

iii) Calculate the dispersion of individual doublons and holons in the magnetic background via the self-consistent Born approximation.

iv) Calculate exciton properties using the Bethe-Salpeter equation.

The major limitation of this program is our approximate description of the magnetic order. Thus we do not claim to have quantitatively accurate results, especially at small magnetization. That said, we do expect that the qualitative trends seen here are accurate, including near the equilibrium value of magnetization, for which mean field theory is known to work reasonably well (see Ref. [45] and references therein).

A. Slave particles

In the slave-particle formalism, we express the electron operator as (with $\sigma = \pm 1$)

$$c_{i\sigma} = s_{i,-\sigma}^\dagger d_i + \sigma e_i^\dagger s_{i\sigma}, \qquad (2)$$

where d_i and e_i are fermionic operators and $s_{i\sigma}$ is bosonic. One can confirm that Eq. (2) is consistent with the commutation relations. A site with a d particle is to be interpreted as a site with two electrons (a "doublon"), a site with an e particle is to be interpreted as an empty site (a "holon"), and a site with an s_σ particle is one with a single electron having spin σ (a "spinon"). See Fig. 2. The physical content of Eq. (2) is then clear: removing an electron of given spin is equivalent to replacing the doublon with the opposite spinon if the site is doubly-occupied and replacing the spinon with a holon
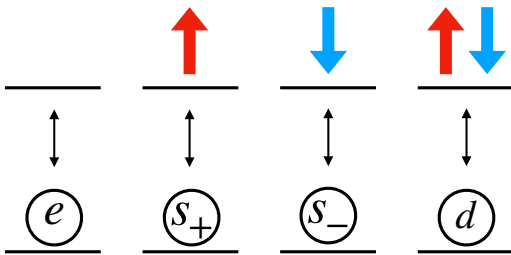
FIG. 2. Sketch of the slave-particle formalism. Each of the four possible occupancies on a site corresponds to a different type of fictitious particle.

if the site is singly-occupied (otherwise the state is annihilated). Note that since every site is in one of the four states – empty, spin-up, spin-down, doubly-occupied – there must be exactly one of the fictitious particles on each site:

$$d_i^\dagger d_i + e_i^\dagger e_i + s_{i\uparrow}^\dagger s_{i\uparrow} + s_{i\downarrow}^\dagger s_{i\downarrow} = 1, \; \forall i. \quad (3)$$

The original Hamiltonian clearly preserves this relationship.

Substituting Eq. (2) into Eq. (1), we have that

$$H_{\text{Hub}} = -t \sum_{\langle ij\rangle,\sigma} \left(d_i^\dagger d_j - e_i^\dagger e_j\right) s_{j\sigma}^\dagger s_{i\sigma} + U \sum_i d_i^\dagger d_i$$
$$- t \sum_{\langle ij\rangle,\sigma} \sigma \left(d_i^\dagger e_j^\dagger s_{i,-\sigma} s_{j\sigma} + e_i d_j s_{i\sigma}^\dagger s_{j,-\sigma}^\dagger\right). \quad (4)$$

Note that the first line preserves the number of doublons and holons, whereas the second line does not.

At large U, the second line of Eq. (4) can be treated by perturbation theory in t/U (starting from states with a definite number of double-occupancies). The method as applied here is standard, and can be found in, e.g., Ref. [61]. We obtain the t-J model:

$$H_{\text{tJ}} = -t \sum_{\langle ij\rangle,\sigma} \left(d_i^\dagger d_j - e_i^\dagger e_j\right) s_{j\sigma}^\dagger s_{i\sigma} + U \sum_i d_i^\dagger d_i$$
$$- J \sum_{\langle ij\rangle} \left(s_{i\uparrow}^\dagger s_{j\downarrow}^\dagger - s_{i\downarrow}^\dagger s_{j\uparrow}^\dagger\right) \left(s_{j\downarrow} s_{i\uparrow} - s_{j\uparrow} s_{i\downarrow}\right), \quad (5)$$

where $J \equiv 4t^2/U$. Strictly speaking, Eq. (5) should include additional next-nearest-neighbor terms, as well as a direct interaction between nearest-neighbor doublons and holons, but these are commonly neglected.

B. Magnetic ordering

The second line of Eq. (5) is precisely the antiferromagnetic Heisenberg Hamiltonian, expressed in terms of Schwinger bosons (here the spinons $s_{i\sigma}$) [61]. We are specifically considering Néel-ordered ground states, with positive magnetization on the A sublattice and negative on B. It is thus convenient to express $s_{i\uparrow}$ ($s_{i\downarrow}$) in terms of $s_{i\downarrow}$ ($s_{i\uparrow}$) for $i \in A$ (B), using Eq. (3) — this is equivalent to using *Holstein-Primakoff* rather than Schwinger bosons [61]:

$$s_{i\uparrow} = \left[1 - s_{i\downarrow}^\dagger s_{i\downarrow}\right]^{1/2}, \quad i \in A,$$
$$s_{i\downarrow} = \left[1 - s_{i\uparrow}^\dagger s_{i\uparrow}\right]^{1/2}, \quad i \in B. \quad (6)$$

We neglect $d_i^\dagger d_i$ and $e_i^\dagger e_i$ in using Eq. (3) because we are interested in the dilute-charge limit. From here on, we shall simply write s_i in place of $s_{i\downarrow}$ ($s_{i\uparrow}$) for $i \in A$ (B). On both sublattices, the s_i boson represents a fluctuation relative to perfect Néel order.

Note that Eq. (6) cannot be an exact equality because it does not respect the fact that $[s_{i\sigma}, s_{i\sigma}^\dagger] = 1$. It is more of a semiclassical approximation, valid in the limit of large spin S. Of course, the case $S = 1/2$ under consideration here is far from large, but all other analytical techniques of which we are aware for treating long-range order via slave particles (such as Bose-Einstein condensation of the Schwinger bosons [62, 63]) have the same regime of validity. We refer to Ref. [61] for more details.

Inserting Eq. (6) into H_{tJ} does not yield a solvable Hamiltonian on its own. Thus to progress further, we make a mean-field approximation by expanding H_{tJ} to first order in $s_i^\dagger s_i - \langle s_i^\dagger s_i\rangle$ (this is also reasonable in the semiclassical limit). With $\langle s_i^\dagger s_i\rangle = 1/2 - m$, where m is the Néel magnetization, we find that

$$H_{\text{tJ}} \approx -\sqrt{\frac{1+2m}{2}} t \sum_{\langle ij\rangle} \left(d_i^\dagger d_j - e_i^\dagger e_j\right) \left(s_i + s_j^\dagger\right)$$
$$+ 4(1+2m)J \sum_i s_i^\dagger s_i + \frac{1+2m}{2} J \sum_{\langle ij\rangle} \left(s_i^\dagger s_j^\dagger + s_i s_j\right)$$
$$+ U \sum_i d_i^\dagger d_i - NJ(1+2m)^2. \quad (7)$$

The second line is diagonalized by passing to momentum space and performing a Bogoliubov transformation, leading to the final Hamiltonian (neglecting constant terms)

$$H_{\text{tJ}} \approx -\sqrt{\frac{1+2m}{2N}} t \sum_{kq} d_{k+q}^\dagger d_k \left(M_{kq}\beta_q + M_{k+q,-q}\beta_{-q}^\dagger\right)$$
$$+ \sqrt{\frac{1+2m}{2N}} t \sum_{kq} e_{k+q}^\dagger e_k \left(M_{kq}\beta_q + M_{k+q,-q}\beta_{-q}^\dagger\right)$$
$$+ U \sum_q d_q^\dagger d_q + \sum_q \omega_q \beta_q^\dagger \beta_q, \quad (8)$$

where the sum is over the 2D Brillouin zone (N is the number of lattice sites) and $\beta_q \equiv u_q s_q + v_q s_{-q}^\dagger$ is the

transformed spinon operator. With

$$u_q \equiv \sqrt{\frac{1}{2}\left(1 + \frac{1}{\sqrt{1-\gamma_q^2}}\right)}, \tag{9}$$

$$v_q \equiv \mathrm{sgn}[\gamma_q]\sqrt{\frac{1}{2}\left(\frac{1}{\sqrt{1-\gamma_q^2}} - 1\right)}, \tag{10}$$

where

$$\gamma_q \equiv \frac{1}{2}\big(\cos q_x + \cos q_y\big), \tag{11}$$

the frequencies ω_q and vertices M_{kq} entering into Eq. (8) are given by

$$\omega_q = 4(1+2m)J\sqrt{1-\gamma_q^2}, \tag{12}$$

$$M_{kq} = 4\gamma_k u_q - 4\gamma_{k+q}v_q. \tag{13}$$

Normally one would determine m self-consistently from the ground state spinon occupation: $1/2 - m = N^{-1}\sum_q \langle s_q^\dagger s_q \rangle = N^{-1}\sum_q v_q^2$. This is known to give $m \approx 0.3$ for a 2D square lattice [45]. We shall instead treat m as an independent parameter — this is an approximate (albeit crude) means of estimating exciton properties as a function of magnetization.

C. Self-consistent Born approximation

The self-consistent Born approximation (SCBA) gives the doublon-doublon and holon-holon propagators by the integral equation in Fig. 3. The same equation holds for each propagator separately. This approximation is expected to be accurate in the dilute-charge limit, where the charge dynamics is strongly affected by spinons but not vice-versa.

In terms of the doublon/holon self-energy $\Sigma_k(\epsilon)$, Fig. 3 translates to (after a frequency integration)

$$\Sigma_k(\epsilon) = \frac{(1+2m)t^2}{2N}\sum_q \frac{M_{kq}^2}{\epsilon - \omega_q - \Sigma_{k-q}(\epsilon - \omega_q)}. \tag{14}$$

The quasiparticle spectrum ϵ_k is given by the solution to $\Sigma_k(\epsilon_k) = \epsilon_k$.

Eq. (14) can be solved quite efficiently. Note that all ω_q are positive [64], thus Eq. (14) in fact expresses $\Sigma_k(\epsilon)$ in terms of the self-energy at lower frequencies. We start at sufficiently negative ϵ, below which we approximate $\Sigma_k(\epsilon) \approx (1+2m)t^2/2N\sum_q M_{kq}^2/(\epsilon - \omega_q)$, and then compute the self-energy at incrementally higher frequencies in terms of the previous values. To help avoid numerical errors, we add a small imaginary part (namely $0.1i(1+2m)J$) to ϵ.
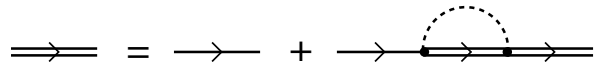

FIG. 3. The self-consistent Born approximation (SCBA) for the single-particle propagator (either doublon-doublon or holon-holon). The solid single line is the free propagator, in this case simply $G_k^0(\epsilon) = 1/\epsilon$, and the solid double line is the full propagator. The dashed line is the spinon propagator and the black dot is the vertex, corresponding to the Hamiltonian in Eq. (8).
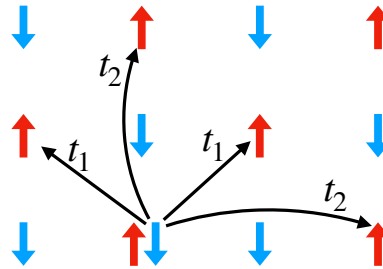

FIG. 4. Illustration of hopping parameters t_1 and t_2 for the approximation to the quasiparticle dispersion in Eq. (15). Singly-occupied sites show the background magnetic order in which the double occupancy hops.

While one could proceed using the full $\Sigma_k(\epsilon)$, it has been found that the quasiparticle dispersion can be well-approximated by the form [65]

$$\begin{aligned}\epsilon_k = &-2t_1\big(\cos(k_x + k_y) + \cos(k_x - k_y)\big)\\ &-2t_2\big(\cos(2k_x) + \cos(2k_y) + 2\big).\end{aligned} \tag{15}$$

This expression has a clear physical interpretation: t_1 is the amplitude for performing a two-step hop along the diagonals of the lattice, and t_2 is the amplitude for a two-step hop along the principal axes (see Fig. 4). Thus in what follows, we shall use for the single-particle propagators the simpler expression

$$G_k(\epsilon) = \frac{1}{\epsilon - (1 - i0)\epsilon_k}, \tag{16}$$

with ϵ_k given by Eq. (15).

D. Bethe-Salpeter equation

We next consider the two-particle Green's function (T denotes time ordering)

$$\begin{aligned}&\mathcal{G}_{j_d j_e; j'_d j'_e}(t_d, t_e; t'_d, t'_e)\\ &\equiv -\langle T d_{j_d}(t_d)e_{j_e}(t_e)e_{j'_e}(t'_e)^\dagger d_{j'_d}(t'_d)^\dagger\rangle,\end{aligned} \tag{17}$$

and its Fourier transform $\mathcal{G}_{k_d k_e; k'_d k'_e}(\epsilon_d, \epsilon_e; \epsilon'_d, \epsilon'_e)$. Due to translational invariance, $\mathcal{G}$ depends only on differences
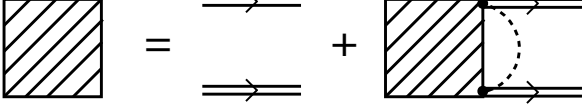
FIG. 5. The integral equation which determines the two-particle Green's function, within the ladder approximation. The hatched square is the Green's function, and all other symbols are as in Fig. 3.

in position and time, which we choose to parametrize by the relative coordinates

$$
\begin{aligned}
j &\equiv j_d - j_e, \\
j' &\equiv j'_d - j'_e, \\
r &\equiv \frac{j_d + j_e}{2} - \frac{j'_d + j'_e}{2},
\end{aligned}
\tag{18}
$$

with relative times defined analogously. The corresponding momenta are

$$
\begin{aligned}
k &= \frac{k_d - k_e}{2}, \\
k' &= \frac{k'_d - k'_e}{2}, \\
K &= k_d + k_e = k'_d + k'_e.
\end{aligned}
\tag{19}
$$

We will use absolute and relative momenta interchangeably, depending on notational convenience, with Eq. (19) always giving the relationship between the two. $\mathcal{G}_{k_d k_e; k'_d k'_e}(\epsilon_d, \epsilon_e; \epsilon'_d, \epsilon'_e)$ will often be written as $\mathcal{G}_{kk'; K}(\epsilon, \epsilon'; E)$.

We determine $\mathcal{G}$ within the ladder approximation as shown in Fig. 5. While admittedly uncontrolled, this approximation does conveniently represent the physics of two-particle bound states being mediated by emission and absorption of spin waves. Written out, the integral equation of Fig. 5 is

$$
\mathcal{G}_{kk'; K}(\epsilon, \epsilon'; E) = G_{k_d}(\epsilon_d) G_{k_e}(\epsilon_e) \left[\delta_{kk'} + \frac{(1+2m)t^2}{2N} \sum_q \int \frac{d\omega}{2\pi i} \left(\frac{M_{k_d-q,q} M_{k_e,q}}{\omega - (1-i0)\omega_q} - \frac{M_{k_d,-q} M_{k_e+q,-q}}{\omega + (1-i0)\omega_q} \right) \mathcal{G}_{k-q, k'; K}(\epsilon-\omega, \epsilon'; E) \right],
\tag{20}
$$

where $G_k(\epsilon)$ is given by Eq. (16) and the vertices M_{kq} are as in Eq. (8).

Since our goal is to identify bound states, we reduce Eq. (20) to the Bethe-Salpeter equation. The details of this approach can be found in Ref. [66]. We assume that $\mathcal{G}$ has an isolated pole in the total energy E, near which it has the form

$$
\mathcal{G}_{kk'; K}(\epsilon, \epsilon'; E) \sim -i \frac{\psi_k(\epsilon) \overline{\psi}_{k'}(\epsilon')}{E - (1-i0)E_b},
\tag{21}
$$

where the "wavefunction" $\psi_k(\epsilon)$, its time-reversed partner $\overline{\psi}_k(\epsilon)$, and the bound state energy E_b remain to be determined. Inserting this ansatz into both sides of Eq. (20) and equating the residues at E_b on each side, we obtain a non-linear eigenvalue problem (the Bethe-Salpeter equation):

$$
\psi_k(\epsilon) = G_{k_d}\left(\frac{E_b}{2} + \epsilon\right) G_{k_e}\left(\frac{E_b}{2} - \epsilon\right) \frac{(1+2m)t^2}{2N} \sum_q \int \frac{d\omega}{2\pi i} \left(\frac{M_{k_d-q,q} M_{k_e,q}}{\omega - (1-i0)\omega_q} - \frac{M_{k_d,-q} M_{k_e+q,-q}}{\omega + (1-i0)\omega_q} \right) \psi_{k-q}(\epsilon - \omega).
\tag{22}
$$

E_b and $\psi_k(\epsilon)$ are given by the solution to Eq. (22). Note that they will depend on the center-of-mass momentum K.

$\psi_k(\epsilon)$ is the bound state wavefunction in a quite literal sense: it is the Fourier transform of

$$
\psi_j(t) = \langle 0 | T d_j(t) e_0(0) | b \rangle,
\tag{23}
$$

where $|b\rangle$ denotes the bound state and $|0\rangle$ denotes the ground state. Note that $t = 0$ is of particular interest, since it gives the amplitude for *simultaneously* observing the holon at site 0 and the doublon at site j. Thus to simplify the problem, we integrate Eq. (22) over ϵ, and furthermore, make the ansatz

$$
\psi_k(\epsilon) = -G_{k_d}\left(\frac{E_b}{2} + \epsilon\right) G_{k_e}\left(\frac{E_b}{2} - \epsilon\right) \left(E_b - \epsilon_{k_d} - \epsilon_{k_e}\right) \Psi_k,
\tag{24}
$$

with Ψ_k independent of ϵ. The explicit factor of $E_b - \epsilon_{k_d} - \epsilon_{k_e}$ is included so that Ψ_k is the equal-time wavefunction, i.e., $\Psi_k = \psi_k(t=0)$. This ansatz allows us to perform the ϵ integral straightforwardly, giving a closed equation for E_b and Ψ_k:

$$
\left(E_b - \epsilon_{k_d} - \epsilon_{k_e}\right) \Psi_k = -\frac{(1+2m)t^2}{2N} \sum_q \left(\frac{M_{k_d-q,q} M_{k_e,q}}{E_b - \epsilon_{k_d-q} - \omega_q - \epsilon_{k_e}} + \frac{M_{k_d,-q} M_{k_e+q,-q}}{E_b - \epsilon_{k_d} - \epsilon_{k_e+q} - \omega_q} \right) \Psi_{k-q}.
\tag{25}
$$

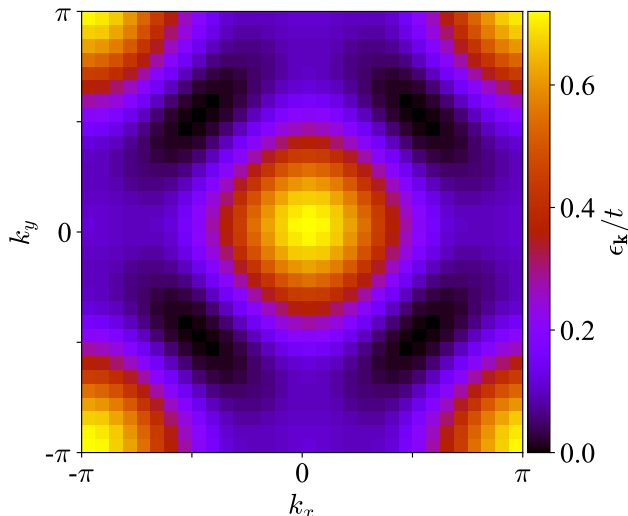Eq. (25) is the two-particle Schrodinger equation albeit with an energy-dependent potential. We find the values

FIG. 6. Dispersion of individual quasiparticles (both doublons and holons) within the SCBA, for a lattice of size 32×32. Data shown is for $t/J = 2$, $m = 0.3$.

of E_b at which it has a non-zero solution, and record the corresponding eigenvector.

Strictly speaking, Eq. (24) is not a valid ansatz for $\psi_k(\epsilon)$, i.e., it does not solve the frequency-dependent Eq. (22). However, it has a clear physical interpretation. The Fourier transform $\psi_k(t)$ gives the wavefunction for inserting the doublon and holon separated by time t (see Eq. (23)). The poles coming from the single-particle propagators in Eq. (24) correspond to the phase factor acquired by the remaining particle during that interval, and our ansatz amounts to neglecting any other time dependence. This approximation has been applied previously to study holon-holon binding [49], and we expect it to be qualitatively accurate for our purposes.

Eq. (25) and those preceding it differ from the equations for holon-holon binding in two respects. First, the holon-holon equations must include exchange terms not found here. Second, due to the relative phase between the doublon-spinon and holon-spinon vertices, the effective potential in Eq. (25) would have the opposite sign for the holon-holon problem.

III. RESULTS

A. Single-particle properties

We first review the behavior of individual quasiparticles, determined within the SCBA as described above. Although these calculations have been reported previously, e.g., in Refs. [59, 65], it will be useful to reproduce them here.

Fig. 6 shows the quasiparticle dispersion throughout the Brillouin zone, with the magnetization set to the
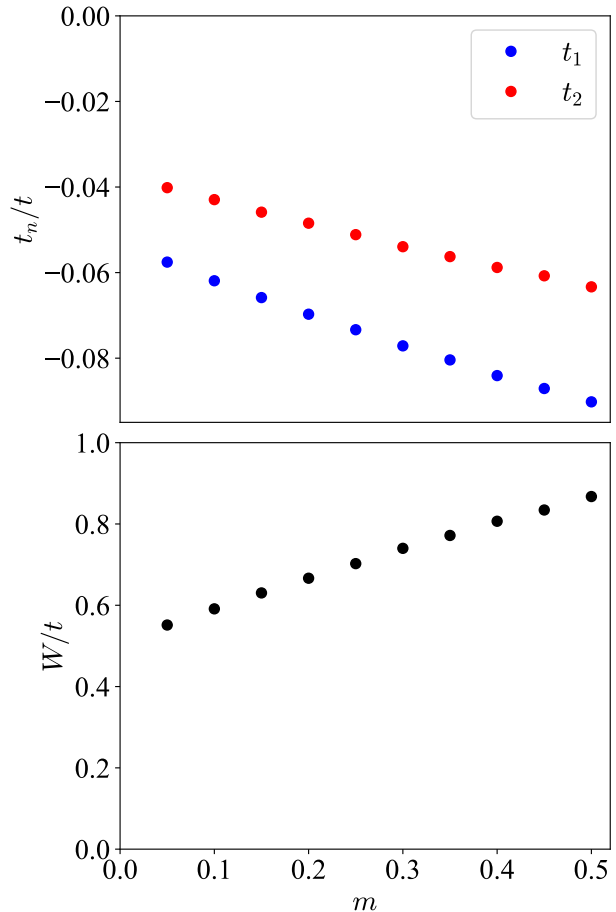

FIG. 7. (Top) Fitted parameters of the quasiparticle dispersion (Eq. (15)) as a function of magnetization, for a lattice of size 32×32 with $t/J = 2$. (Bottom) Quasiparticle bandwidth versus magnetization for the same system.

equilibrium value for concreteness. As noted above, it can be well-approximated by a next-nearest-neighbor hopping model with amplitude t_1 for moving along the diagonals of the lattice and amplitude t_2 for moving along the principal axes (see Fig. 4). The form of the dispersion is not sensitive to the value of magnetization. However, the effective hopping amplitudes, which we determine empirically by fitting the computed spectrum to Eq. (15), do depend on m as shown in Fig. 7.

Some features of the dispersion can be explained by a simple Hartree-Fock approximation to the original Hamiltonian, in which the Hubbard interaction is replaced by $n_{i\uparrow}\langle n_{i\downarrow}\rangle + \langle n_{i\uparrow}\rangle n_{i\downarrow}$. Assuming Néel order for $\langle n_{i\sigma}\rangle$, the Hamiltonian becomes a tight-binding model on a bipartite lattice with dispersion

$$
\begin{aligned}
\epsilon_k^{(\mathrm{HF})} &= \sqrt{U^2 + 4t^2\big(\cos k_x + \cos k_y\big)^2} \\
&\sim U + \frac{2t^2}{U}\big(\cos k_x + \cos k_y\big)^2,
\end{aligned}
\tag{26}
$$

using that $t \ll U$. Up to a constant shift, the second line is equivalent to Eq. (15) for the special case $t_1 = 2t_2$. Note in particular that $t_1, t_2 < 0$. Thus Hartree-Fock correctly predicts that the band minimum is within the lines $k_k + k_y = \pm\pi$. It also correctly suggests that the bandwidth should be significantly reduced to $O(J)$ instead of $O(t)$. However, it *incorrectly* claims that the dispersion is degenerate along the entire magnetic Brillouin zone boundary. The more sophisticated SCBA resolves this degeneracy, identifying four minima at $(k_x, k_y) = (\pm\pi/2, \pm\pi/2)$.

Recent work on magnetic polarons in the t-J model [67, 68] has made clear that this behavior can be understood by the charge excitations forming spinon-charge bound states (the "polarons"), held together by strings of displaced spins (much as we have sketched in Fig. 1 but with individual charges). The charges are forced to move on the timescale set by their slower spinon partners, namely $O(1/J)$, and are subject to the bipartite lattice felt by the spinons. The dispersion results shown above confirm this string picture quite nicely if one interprets them as being for the *polaron* as a whole. With that in mind, it is rather striking that these three approaches — SCBA, Hartree-Fock, and the string picture — all lead to consistent conclusions.

Returning to Fig. 7, we see that the bandwidth W increases noticeably as the magnetization increases. Equivalently, the single-particle mass decreases. Within the framework of our calculation, the explanation is clear: a doublon/holon can move only if a spinon takes its place (see Eq. (5)), and since one spinon factor is always in the direction of the Néel magnetization, the doublon/holon hopping term is proportional to $\sqrt{(1+2m)/2}$.

B. Exciton properties

We now turn to the exciton properties as functions of magnetization, using the Bethe-Salpeter equation. All of the quantities presented here are straightforward to compute from the energy E_b and wavefunction ψ_k given by Eq. (22).

Fig. 8 shows the energy of the lowest internal state as a function of the center-of-mass momentum K. As was the case for the single-particle dispersion, the shape of the exciton dispersion is not particularly sensitive to the magnetization. Note that the bottom of the band is not at the origin but rather at $(K_x, K_y) = (\pi, \pi)$. The wavefunction of the (π, π) state is shown in Fig. 9. We leave for future work a full group-theoretic classification of the exciton wavefunctions based on square-lattice symmetry, including the selection rules for creating Mott excitons, but we expect that it can be carried out straightforwardly — for example, the wavefunction in Fig. 9 has s-wave symmetry about the point $(\pi/2, \pi/2)$ (which is the high-symmetry point of Eq. (25)).

The binding energy, mass, and radius of the exciton are plotted versus magnetization in Fig. 10. We see that
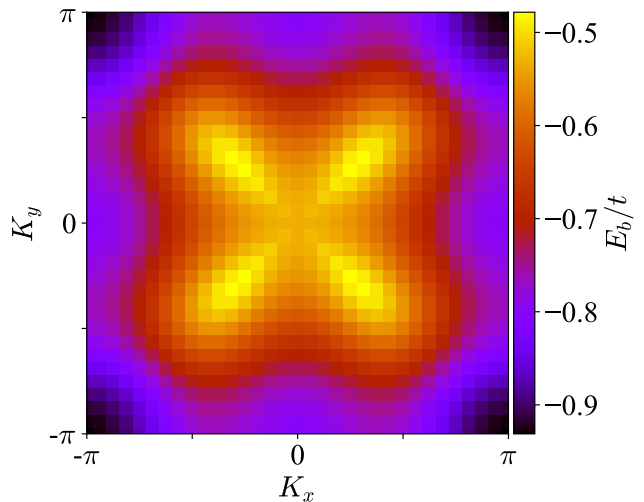

FIG. 8. Dispersion of the exciton center-of-mass motion, for a lattice of size 32×32. Data shown is for $t/J = 2$, $m = 0.3$.

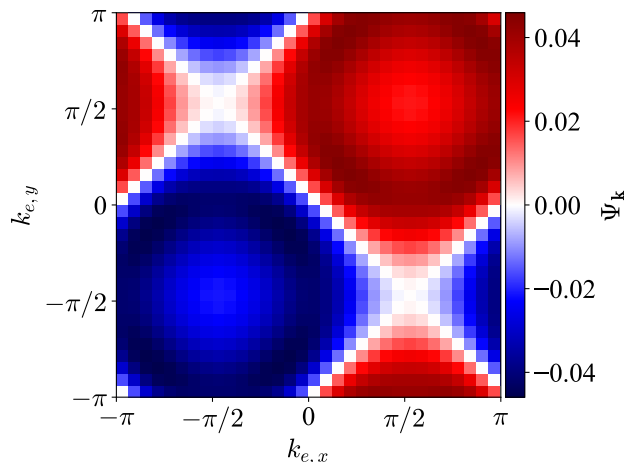

FIG. 9. Exciton wavefunction in (relative) momentum space at total momentum $(K_x, K_y) = (\pi, \pi)$, for the same system as in Fig. 8.

as one increases the magnetization m, the mass decreases while the binding energy and size increase. It is interesting to compare these trends with what one would expect for a conventional exciton formed via Coulomb attraction. In that situation, a decrease in mass is associated with an increase in radius and a decrease in binding energy. Here, we find a similar relationship between radius and mass, but the binding energy instead scales *inversely* with mass.

Eq. (25) can be simplified further in the large-t/J limit. We will see that E_b scales as t, whereas ϵ_k and ω_q are asymptotically smaller [65]. Thus we can neglect the single-particle and spinon dispersions, leaving the equa-
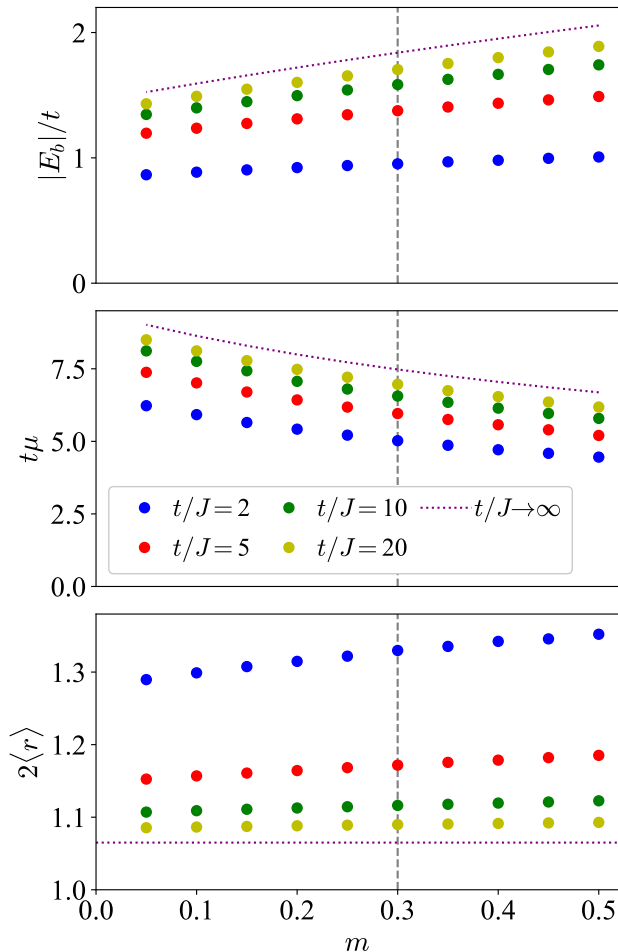
FIG. 10. Exciton properties as functions of magnetization m, for various t/J and a lattice of size 32×32. The $t/J \to \infty$ curves are obtained from Eq. (27). Vertical dashed lines indicate the equilibrium value of m. (Top) Binding energy. (Center) Mass. (Bottom) Diameter.
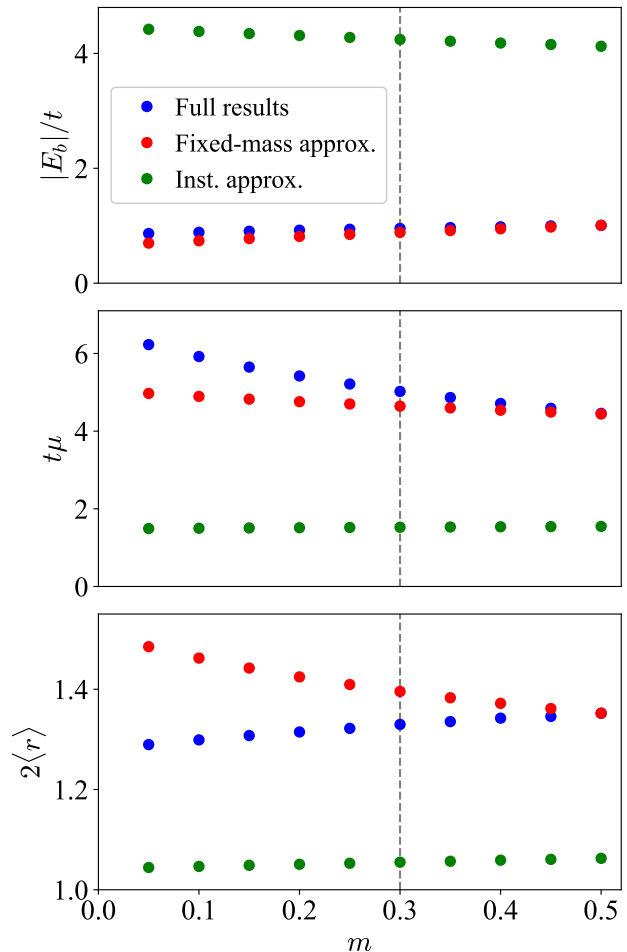

FIG. 11. Comparison between the full results and the two approximations considered in the text. Data shown is for $t/J = 2$ and a lattice of size 32×32. Vertical dashed lines indicate the equilibrium value of m. For the fixed-mass points, the values of t_1 and t_2 are set to their values at $m = 0.5$ (see Fig. 7).

tion

$$E_b^2 \Psi_k = - \frac{(1+2m)t^2}{2N} \sum_q \big(M_{k_d-q,q} M_{k_e,q}$$
$$+ M_{k_d,-q} M_{k_e+q,-q} \big) \Psi_{k-q}. \tag{27}$$

Although still not of the Schrodinger form, Eq. (27) is much simpler to solve than Eq. (25): the kernel on the right-hand side no longer depends self-consistently on the energy (and as claimed, $E_b \sim t$). The results obtained from the large-t/J equation are plotted alongside the others in Fig. 10.

As is clear from Eq. (25), the spinon-mediated interaction between charges is not instantaneous. To assess the importance of this retardation, we have compared the results in Fig. 10 to what would be obtained through the static approximation (setting $\omega = 0$ in the kernel of Eq. (22)). The static approximation would predict sig-

nificantly different results, as seen in Fig. 11: the binding energy would instead decrease slightly with magnetization and the mass would increase slightly. Thus the retardation of the effective interaction is an essential ingredient to the behavior seen here.

Similarly, one can ask whether the trends observed in Fig. 10 are due primarily to changes in the spinon behavior or rather due to the *single*-particle mass, which itself decreases with magnetization. We have repeated the above calculations under "fixed-mass" conditions, in which the single-particle parameters t_1 and t_2 are kept fixed (to their values at $m = 0.5$) as we vary the magnetization. Fig. 11 shows that each of the three observables responds differently. The binding energy becomes more sensitive to magnetization, indicating that the quasiparticle and spinon properties play antagonistic roles. On the other hand, the exciton mass becomes less sensitive – the change to the effective interaction suppresses the

mass by itself. Finally, the exciton radius shows the reverse behavior to before, instead decreasing with magnetization (although the size remains quite small in absolute terms).

Certain trends seen here are somewhat surprising. For example, we find that the exciton radius increases with increasing magnetization, but one might have expected it to decrease. The fixed-mass calculation provides a partial explanation: the spin waves on their own do in fact force the charges closer together at larger magnetization, but this effect is overcompensated by each individual charge becoming lighter. Whether the charges becoming lighter is itself a real effect or rather an artifact of our approximations is less clear, and something that warrants further investigation.

It is also surprising that the exciton binding energy does not vanish as $J/t \to 0$, since the binding is mediated by spin waves in the first place. While more systematic studies are clearly needed, this does not strike us as necessarily contradictory. Keep in mind that we are considering the behavior of a single doublon-holon pair on top of an antiferromagnetically ordered background. Setting $J = 0$ does not change the fact that our initial state is ordered, nor that the motion of charges disturbs that order — in the slave-particle language, the spinons are inert at $J = 0$ but the hopping of a charge does still leave a string of spin excitations in its wake (see Eq. (7)). It is conceivable that interference effects analogous to Nagaoka ferromagnetism [61, 69] (whereby background ferromagnetic order lowers the energy of a single hole by $O(t)$ even at $J = 0$) could bind pairs of charges together in an antiferromagnetic background as well, implying $E_b = O(t)$. Further investigation is certainly warranted, however.

One final surprise is that the binding energy does not vanish at $m = 0$ either, but this we fully expect to be an artifact of our approximations. We have treated the magnetic order along the lines of spin wave theory — this is most justified at full magnetization, and seems to work well at the equilibrium magnetization [45], but fails at $m = 0$. We do not see the failure at $m = 0$ as invalidating the trends found for larger magnetization, however.

The recent pump-probe experiments in Refs. [29, 30] have investigated how excitons are influenced by magnetic order in the Mott insulator Na_2IrO_3. Our results support their interpretation in some aspects but not in others. In Ref. [29], the authors observe an increase in the fraction of bound excitations when below the Néel temperature, which they attribute to an increase in the exciton binding energy. Fig. 10 shows that magnetic order does indeed increase the binding energy. On the other hand, Ref. [30] demonstrates that the relaxational dynamics following a pump are slower in the presence of magnetic order. This is attributed to the mass increasing with magnetization, yet we have observed the opposite (consistent with past works calculating the dependence on J/t [60, 65, 70]). Given the highly non-equilibrium nature of the experiments, as well as the approximations inherent in an analytical approach, further investigation is clearly needed.

Lastly, let us compare the present calculation of doublon-holon binding to that of holon-holon binding, which is obviously of significant interest in its own right [58, 71]. Clearly the two have much in common, yet there are two important differences. First, the integral equation which determines the two-particle Green's function (Fig. 5) has an additional exchange term due to the indistinguishability of the holons. Second, even the direct term comes with an extra minus sign, i.e., the effective interaction is of opposite sign. The sign can be removed by redefining the hole operator on one sublattice, but the additional phase may modify further results depending on the application. It is important to keep these distinctions in mind when relating the present results to the high-T_c literature.

IV. CONCLUSION

We have studied the role that magnetic order plays in the formation of excitons within Mott insulators, using the Hubbard model as a concrete (albeit simplified) Hamiltonian. The binding energy increases in the presence of antiferromagnetic magnetization, whereas the exciton mass decreases. The size of the exciton increases slightly, yet the radius is never more than a lattice spacing. Using the standard classification, these are Frenkel excitons regardless of magnetic order.

In addition, we have established that the trends observed here require a detailed understanding of the many-body dynamics in these systems. Retardation effects in the effective spinon-mediated interaction are essential. Furthermore, the constituent charge and spin excitations are each affected separately by the background magnetic order, in ways cooperative for some exciton properties but antagonistic for others.

It must be noted that despite the complexity, there are significant limitations to our approach. In particular, we have made approximations in the spirit of linear spin-wave theory, which is only justified at large spin S and full magnetization (neither of which we assume here). Thus we do not expect these results to be quantitatively accurate — we instead view this analysis as expressing our physical intuition regarding Mott excitons in the language of slave particles, from which we can make sharp predictions to be verified or falsified by more systematic investigations.

As an outlook, the predictions made here will be important when analyzing recent and future experiments on the optical properties of strongly correlated electronic materials. The existing experiments are quite complex, and require interpretations of their own. Our results agree with those interpretations in some respects but disagree in others. A complete understanding of the systems will require many approaches, both experimental and theoretical, including but not limited to the one de-

scribed here.

Particularly promising are the recent experiments on fermionic atoms in optical lattices [41, 42, 44]. Since ultracold gases do not have many of the complicating features found in condensed matter systems, we expect that this will be a valuable direction to explore further. It is also likely that our conclusions, being based on the single-band nearest-neighbor Hubbard model, are more applicable to those systems than to materials such as the iridates. Importantly, current quantum gas microscopes allow one to directly create localized doublons and holons via optical tweezers, and reliably measure the spin correlation functions [43]. Such an unprecedented direct access to the system microscopics will provide a powerful way of investigating many-body excitons.

V. ACKNOWLEDGEMENTS

[1] H. Haug and S. Schmitt-Rink, "Electron theory of the optical properties of laser-excited semiconductors," Progress in Quantum Electronics **9**, 3 – 100 (1984).

[2] H. Haug and S. W. Koch, *Quantum Theory of the Optical and Electronic Properties of Semiconductors* (World Scientific, 2004).

[3] J. H. Burroughes, D. D. C. Bradley, A. R. Brown, R. N. Marks, K. Mackay, R. H. Friend, P. L. Burns, and A. B. Holmes, "Light-emitting diodes based on conjugated polymers," Nature **347**, 539–541 (1990).

[4] Brian A. Gregg, "Excitonic solar cells," The Journal of Physical Chemistry B **107**, 4688–4698 (2003).

[5] Mikhail E. Itkis, Ferenc Borondics, Aiping Yu, and Robert C. Haddon, "Bolometric infrared photoresponse of suspended single-walled carbon nanotube films," Science **312**, 413–416 (2006).

[6] Iacopo Carusotto and Cristiano Ciuti, "Quantum fluids of light," Rev. Mod. Phys. **85**, 299–366 (2013).

[7] J. Kasprzak, M. Richard, S. Kundermann, A. Baas, P. Jeambrun, J. M. J. Keeling, F. M. Marchetti, M. H. Szymańska, R. André, J. L. Staehli, V. Savona, P. B. Littlewood, B. Deveaud, and Le Si Dang, "Bose–einstein condensation of exciton polaritons," Nature **443**, 409–414 (2006).

[8] J Keeling, F M Marchetti, M H Szymańska, and P B Littlewood, "Collective coherence in planar semiconductor microcavities," Semiconductor Science and Technology **22**, R1–R26 (2007).

[9] Hui Deng, Hartmut Haug, and Yoshihisa Yamamoto, "Exciton-polariton bose-einstein condensation," Rev. Mod. Phys. **82**, 1489–1537 (2010).

[10] Tim Byrnes, Na Young Kim, and Yoshihisa Yamamoto, "Exciton–polariton condensates," Nature Physics **10**, 803 EP – (2014).

[11] Johannes D. Plumhof, Thilo Stöferle, Lijian Mai, Ullrich Scherf, and Rainer F. Mahrt, "Room-temperature bose–einstein condensation of cavity exciton–polaritons in a polymer," Nature Materials **13**, 247–252 (2014).

[12] F. B. Gallagher and S. Mazumdar, "Excitons and optical absorption in one-dimensional extended hubbard models with short- and long-range interactions," Phys. Rev. B **56**, 15025–15039 (1997).

[13] H. S. Choi, Y. S. Lee, T. W. Noh, E. J. Choi, Yunkyu Bang, and Y. J. Kim, "Anomalous temperature dependence of charge-transfer excitation in the undoped cuprate $sr_2cuo_2cl_2$," Phys. Rev. B **60**, 4646–4652 (1999).

[14] Eiichi Hanamura, Nguyen Trung Dan, and Yukito Tanabe, "Excitons and two-magnon raman scattering of the strongly correlated systems la_2cuo_4 and $yba_2cu_3o_6$," Phys. Rev. B **62**, 7033–7044 (2000).

[15] F. H. L. Essler, F. Gebhard, and E. Jeckelmann, "Excitons in one-dimensional mott insulators," Phys. Rev. B **64**, 125119 (2001).

[16] P. Wróbel and R. Eder, "Excitons in mott insulators," Phys. Rev. B **66**, 035111 (2002).

[17] T. Tohyama, H. Onodera, K. Tsutsui, and S. Maekawa, "Resonant two-magnon raman scattering and photoexcited states in two-dimensional mott insulators," Phys. Rev. Lett. **89**, 257405 (2002).

[18] A. Maeda, M. Ono, H. Kishida, T. Manako, A. Sawa, M. Kawasaki, Y. Tokura, and H. Okamoto, "Third-order nonlinear susceptibility spectra of CuO chain compounds investigated by the z-scan method," Phys. Rev. B **70**, 125117 (2004).

[19] H. Matsueda, T. Tohyama, and S. Maekawa, "Excitonic effect on the optical response in the one-dimensional two-band hubbard model," Phys. Rev. B **71**, 153106 (2005).

[20] M. Ono, H. Kishida, and H. Okamoto, "Direct observation of excitons and a continuum of one-dimensional mott insulators: A reflection-type third-harmonic-generation study of ni-halogen chain compounds," Phys. Rev. Lett. **95**, 087401 (2005).

[21] T. Tohyama, "Symmetry of photoexcited states and large-shift raman scattering in two-dimensional mott insulators," Journal of the Physical Society of Japan **75**, 034713 (2006).

[22] A. Gössling, R. Schmitz, H. Roth, M. W. Haverkort, T. Lorenz, J. A. Mydosh, E. Müller-Hartmann, and M. Grüninger, "Mott-hubbard exciton in the optical conductivity of ytio$_3$ and smtio$_3$," Phys. Rev. B **78**, 075122 (2008).

[23] K. A. Al-Hassanieh, F. A. Reboredo, A. E. Feiguin, I. González, and E. Dagotto, "Excitons in the one-dimensional hubbard model: A real-time study," Phys. Rev. Lett. **100**, 166403 (2008).

[24] Fabio Novelli, Daniele Fausti, Julia Reul, Federico Cilento, Paul H. M. van Loosdrecht, Agung A. Nugroho, Thomas T. M. Palstra, Markus Grüninger, and Fulvio Parmigiani, "Ultrafast optical spectroscopy of the lowest energy excitations in the mott insulator compound yvo$_3$: Evidence for hubbard-type excitons," Phys. Rev. B **86**, 165135 (2012).

[25] H. Gretarsson, J. P. Clancy, X. Liu, J. P. Hill, Emil Bozin, Yogesh Singh, S. Manni, P. Gegenwart, Jungho Kim, A. H. Said, D. Casa, T. Gog, M. H. Upton, Heung-Sik Kim, J. Yu, Vamshi M. Katukuri, L. Hozoi, Jeroen van den Brink, and Young-June Kim, "Crystal-field splitting and correlation effect on the electronic structure of A_2iro$_3$," Phys. Rev. Lett. **110**, 076402 (2013).

[26] Zala Lenarcic and Peter Prelovsek, "Ultrafast charge recombination in a photoexcited mott-hubbard insulator," Phys. Rev. Lett. **111**, 016401 (2013).

[27] Jungho Kim, M. Daghofer, A. H. Said, T. Gog, J. van den Brink, G. Khaliullin, and B. J. Kim, "Excitonic quasiparticles in a spin–orbit mott insulator," Nature Communications **5**, 4453 (2014).

[28] Sen Zhou, Yupeng Wang, and Ziqiang Wang, "Doublon-holon binding, mott transition, and fractionalized antiferromagnet in the hubbard model," Phys. Rev. B **89**, 195119 (2014).

[29] Zhanybek Alpichshev, Fahad Mahmood, Gang Cao, and Nuh Gedik, "Confinement-deconfinement transition as an indication of spin-liquid-type behavior in na$_2$iro$_3$," Phys. Rev. Lett. **114**, 017203 (2015).

[30] Zhanybek Alpichshev, Edbert J. Sie, Fahad Mahmood, Gang Cao, and Nuh Gedik, "Origin of the exciton mass in the frustrated mott insulator na$_2$iro$_3$," Phys. Rev. B **96**, 235141 (2017).

[31] T. Terashige, T. Ono, T. Miyamoto, T. Morimoto, H. Yamakawa, N. Kida, T. Ito, T. Sasagawa, T. Tohyama, and H. Okamoto, "Doublon-holon pairing mechanism via exchange interaction in two-dimensional cuprate mott insulators," Science Advances **5** (2019).

[32] Martin Eckstein and Philipp Werner, "Ultra-fast photo-carrier relaxation in mott insulators with short-range spin correlations," Scientific Reports **6**, 21235 (2016).

[33] U. Schneider, L. Hackermüller, S. Will, Th. Best, I. Bloch, T. A. Costi, R. W. Helmes, D. Rasch, and A. Rosch, "Metallic and insulating phases of repulsively interacting fermions in a 3d optical lattice," Science **322**, 1520–1525 (2008).

[34] Immanuel Bloch, Jean Dalibard, and Wilhelm Zwerger, "Many-body physics with ultracold gases," Rev. Mod. Phys. **80**, 885–964 (2008).

[35] Tilman Esslinger, "Fermi-hubbard physics with atoms in an optical lattice," Annual Review of Condensed Matter Physics **1**, 129–152 (2010).

[36] Immanuel Bloch, Jean Dalibard, and Sylvain Nascimbène, "Quantum simulations with ultracold quantum gases," Nature Physics **8**, 267–276 (2012).

[37] Christian Gross and Immanuel Bloch, "Quantum simulations with ultracold atoms in optical lattices," Science **357**, 995 (2017).

[38] Maxwell F. Parsons, Anton Mazurenko, Christie S. Chiu, Geoffrey Ji, Daniel Greif, and Markus Greiner, "Site-resolved measurement of the spin-correlation function in the fermi-hubbard model," Science **353**, 1253 (2016).

[39] Martin Boll, Timon A. Hilker, Guillaume Salomon, Ahmed Omran, Jacopo Nespolo, Lode Pollet, Immanuel Bloch, and Christian Gross, "Spin- and density-resolved microscopy of antiferromagnetic correlations in fermi-hubbard chains," Science **353**, 1257 (2016).

[40] Lawrence W. Cheuk, Matthew A. Nichols, Katherine R. Lawrence, Melih Okan, Hao Zhang, Ehsan Khatami, Nandini Trivedi, Thereza Paiva, Marcos Rigol, and Martin W. Zwierlein, "Observation of spatial charge and spin correlations in the 2d fermi-hubbard model," Science **353**, 1260 (2016).

[41] Timon A. Hilker, Guillaume Salomon, Fabian Grusdt, Ahmed Omran, Martin Boll, Eugene Demler, Immanuel Bloch, and Christian Gross, "Revealing hidden antiferromagnetic correlations in doped hubbard chains via string correlators," Science **357**, 484 (2017).

[42] Guillaume Salomon, Joannis Koepsell, Jayadev Vijayan, Timon A. Hilker, Jacopo Nespolo, Lode Pollet, Immanuel Bloch, and Christian Gross, "Direct observation of incommensurate magnetism in hubbard chains," Nature **565**, 56–60 (2019).

[43] Joannis Koepsell, Jayadev Vijayan, Pimonpan Sompet, Fabian Grusdt, Timon A. Hilker, Eugene Demler, Guillaume Salomon, Immanuel Bloch, and Christian Gross, "Imaging magnetic polarons in the doped fermi–hubbard model," Nature **572**, 358–362 (2019).

[44] Jayadev Vijayan, Pimonpan Sompet, Guillaume Salomon, Joannis Koepsell, Sarah Hirthe, Annabelle Bohrdt, Fabian Grusdt, Immanuel Bloch, and Christian Gross, "Time-resolved observation of spin-charge deconfinement in fermionic hubbard chains," Science **367**, 186 (2020).

[45] Xing-Jie Han, Yu Liu, Zhi-Yuan Liu, Xin Li, Jing Chen, Hai-Jun Liao, Zhi-Yuan Xie, B Normand, and Tao Xiang, "Charge dynamics of the antiferromagnetically ordered mott insulator," New Journal of Physics **18**, 103004 (2016).

[46] Boris I. Shraiman and Eric D. Siggia, "Mean-field theory for vacancies in a quantum antiferromagnet," Phys. Rev. B **40**, 9162–9166 (1989).

[47] M. Yu. Kuchiev and O. P. Sushkov, "Large-size two-hole bound states in the t-j model," Physica C: Superconductivity **218**, 197–207 (1993).

[48] V. I. Belinicher, A. L. Chernyshev, A. V. Dotsenko, and O. P. Sushkov, "Hole-hole superconducting pairing in the t-j model induced by spin-wave exchange," Phys. Rev. B **51**, 6076–6084 (1995).

[49] V. I. Belinicher, A. L. Chernyshev, and V. A. Shubin, "Two-hole problem in the t-j model: A canonical transformation approach," Phys. Rev. B **56**, 3381–3393 (1997).

[50] C. Brügger, F. Kämpfer, M. Pepe, and U. J. Wiese, "Magnon-mediated binding between holes in an antifer-

romagnet." European Physical Journal B – Condensed Matter **53**, 433–437 (2006).

[51] J. E. Hirsch, "Two-dimensional hubbard model: Numerical simulation study," Phys. Rev. B **31**, 4403–4419 (1985).

[52] Gabriel Kotliar and Andrei E. Ruckenstein, "New functional integral approach to strongly correlated fermi systems: The gutzwiller approximation as a saddle point," Phys. Rev. Lett. **57**, 1362–1365 (1986).

[53] S. R. White, D. J. Scalapino, R. L. Sugar, E. Y. Loh, J. E. Gubernatis, and R. T. Scalettar, "Numerical study of the two-dimensional hubbard model," Phys. Rev. B **40**, 506–516 (1989).

[54] Patrick A. Lee, "Gauge field, aharonov-bohm flux, and high-T_c superconductivity," Phys. Rev. Lett. **63**, 680–683 (1989).

[55] Tohru Ogawa, Kunihiko Kanda, and Takeo Matsubara, "Gutzwiller approximation for antiferromagnetism in hubbard model *)," Progress of Theoretical Physics **53**, 614–633 (1975).

[56] A. H. MacDonald, S. M. Girvin, and D. Yoshioka, "$\frac{t}{U}$ expansion for the hubbard model," Phys. Rev. B **37**, 9753–9756 (1988).

[57] T. Li, P. Wölfle, and P. J. Hirschfeld, "Spin-rotation-invariant slave-boson approach to the hubbard model," Phys. Rev. B **40**, 6817–6821 (1989).

[58] Patrick A. Lee, Naoto Nagaosa, and Xiao-Gang Wen, "Doping a mott insulator: Physics of high-temperature superconductivity," Rev. Mod. Phys. **78**, 17–85 (2006).

[59] S. Schmitt-Rink, C. M. Varma, and A. E. Ruckenstein, "Spectral function of holes in a quantum antiferromagnet," Phys. Rev. Lett. **60**, 2793–2796 (1988).

[60] C. L. Kane, P. A. Lee, and N. Read, "Motion of a single hole in a quantum antiferromagnet," Phys. Rev. B **39**, 6880–6897 (1989).

[61] A. Auerbach, *Interacting Electrons and Quantum Magnetism* (Springer, 1994).

[62] Sanjoy Sarker, C. Jayaprakash, H. R. Krishnamurthy, and Michael Ma, "Bosonic mean-field theory of quantum heisenberg spin systems: Bose condensation and magnetic order," Phys. Rev. B **40**, 5028–5035 (1989).

[63] Sanjoy K. Sarker, H.R. Krishnamurthy, C. Jayaprakash, and W. Wenzel, "Mean-field theories of hubbard and t-j models," Physica B: Condensed Matter **163**, 541 – 543 (1990).

[64] More precisely, all ω_q are non-negative, but the vertex vanishes on those momenta such that $\omega_q = 0$.

[65] Gerardo Martinez and Peter Horsch, "Spin polarons in the t-j model," Phys. Rev. B **44**, 317–331 (1991).

[66] Noboru Nakanishi, "A general survey of the theory of the bethe-salpeter equation," Progress of Theoretical Physics Supplement **43**, 1–81 (1969).

[67] Fabian Grusdt, Annabelle Bohrdt, and Eugene Demler, "Microscopic spinon-chargon theory of magnetic polarons in the $t-j$ model," Phys. Rev. B **99**, 224422 (2019).

[68] Annabelle Bohrdt, Eugene Demler, Frank Pollmann, Michael Knap, and Fabian Grusdt, "Parton theory of angle-resolved photoemission spectroscopy spectra in antiferromagnetic mott insulators," Phys. Rev. B **102**, 035139 (2020).

[69] Y. Nagaoka, "Ferromagnetism in a narrow, almost half-filled s band," Phys. Rev. **147**, 392–405 (1966).

[70] K. J. von Szczepanski, P. Horsch, W. Stephan, and M. Ziegler, "Single-particle excitations in a quantum antiferromagnet," Phys. Rev. B **41**, 2017–2029 (1990).

[71] N. Plakida, *High-Temperature Cuprate Superconductors: Experiment, Theory, and Applications* (Springer Berlin Heidelberg, 2010).